



Effects of Water Saturation and Loading Condition on Rock Tensile Strength: Insights from Acoustic Emission Analysis

Jun Zhu^{1,2} · Jianhui Deng^{2,3} · Po Ning¹ · Ziguo Fu³ · Xuankun Li³ · Ronald Y. S. Pak⁴

Received: 4 June 2023 / Accepted: 8 September 2023 / Published online: 3 October 2023
© The Author(s), under exclusive licence to Springer-Verlag GmbH Austria, part of Springer Nature 2023

Abstract

The tensile strength of rocks is affected by loading conditions, specifically direct and Brazilian tension, as well as water saturation. But the fundamental reasons for the differences between direct tensile strength σ_{td} and Brazilian tensile strength σ_{tb} , and their degradation induced by water saturation, are not yet fully understood. Here, we report a series of direct tensile and Brazilian tests performed on marble and granite rocks under both dry and water-saturated conditions. We employed the acoustic emission (AE) technique and further analyzed the recorded AE waveforms using a methodology based on the statistical analysis of dominant frequency to infer the intrinsic failure process of studied rocks under different water and loading conditions. Our results show that water saturation causes substantial reductions in both σ_{td} and σ_{tb} , with the reduction in σ_{tb} being greater. A correspondence between AE waveforms distributed in high and low dominant frequency bands (H-type and L-type waveform) and rock failure types is found, that is, the H-type waveforms correspond to the micro-shear failures, and the L-type waveforms correspond to the micro-tensile failures. Based on this, the generation of abundant micro-shear failures is the cause of enhancement in σ_{tb} in rocks compared to its σ_{td} , and the reductions in σ_{td} and σ_{tb} for saturated rocks result from increasing micro-tensile failures. Furthermore, the friction-weakening effect induced by lubricating water films is responsible for the tensile strength reduction of saturated marble and granite under direct and Brazilian tension. The pronounced friction-weakening effect resulting from the widespread friction condition in the Brazilian test facilitates the σ_{tb} loss. In addition to the friction-weakening effect, stress corrosion could also be a secondary cause of the tensile strength reduction of saturated granite.

Highlights

- The corresponding relationship between acoustic emission waveform types with micro-failure patterns is built.
- Reasons for the difference in measured tensile strength under direct and Brazilian tension are proposed.
- Water-weakening effects on the tensile strength of rocks under direct tension and Brazilian loading are revealed.

Keywords Tensile strength · Water saturation · Loading condition · Acoustic emission (AE) · Dominant frequency · Failure type

✉ Jianhui Deng
jhdeng@scu.edu.cn

¹ Key Laboratory of Mountain Hazards and Earth Surface Process, Institute of Mountain Hazards and Environment, Chinese Academy of Sciences (CAS), Chengdu 610299, China

² Key Laboratory of Deep Earth Science and Engineering (Sichuan University), Ministry of Education, Chengdu 610065, China

³ State Key Laboratory of Hydraulics and Mountain River Engineering, College of Water Resources and Hydropower, Sichuan University, Chengdu 610065, China

⁴ Department of Civil, Environmental and Architectural Engineering, University of Colorado, Boulder, CO 80309, USA

List of Symbols

σ_t	Tensile strength
σ_{td}	Direct tensile strength, DTS
σ_{tb}	Brazilian tensile strength, BTS
P	Applied peak load
A	Cross-sectional area of the cylinder
D	Diameter of the Brazilian disk
T	Thickness of the Brazilian disk
k	Ratio of the RA value and AF value
P_H	Percentage of H-type waveform
P_L	Percentage of L-type waveform
P_{EH}	Energy ratio of H-type waveform
P_{EL}	Energy ratio of L-type waveform
χ	Ratio of the Brazilian tensile strength and direct tensile strength

1 Introduction

Among the various environmental factors affecting rock mechanical properties, water is widely recognized as the most usual and intractable trouble to engineers. Rock strength degradation induced by water saturation may trigger a large number of geotechnical disasters, such as landslides (Song et al. 2018), ground subsidence (Bajni et al. 2019), and fault activation (Dang et al. 2019; Ma et al. 2019). It is then crucial to understand the water–rock interaction effects on rock strength to assess and prevent engineering problems in water environments.

In recent decades, substantial efforts have been devoted to evaluating the water-weakening effects on various strength properties of rocks, including uniaxial compressive strength, elastic modulus, tensile strength, and shear strength, of various rock types (Hashiba and Fukui 2015; Jiang et al. 2014; Rabat et al. 2020a, 2022). It is generally accepted that water saturation causes the rock strength properties to be weak, and the extent of this weakening effect mainly depends on the rock type. Among these rock strength properties mentioned above, tensile strength is of immense significance and is currently a topic in vogue; this is because many rock mass in engineering practices, e.g., basements, caverns, and diversion tunnels of hydro-power stations, is subject to tension and they are much weaker in tension than in compression. Therefore, a comprehensive understanding of the water–rock interaction effects on rock tensile strength is urgent for engineers.

Several alternative methods, classified into direct and indirect methods, could be used to measure the tensile strength of rock. In 1978, the standard published by the International Society for Rock Mechanics (ISRM) outlined the execution details of the direct tensile test and the

Brazilian test (ISRM 1978). Direct tensile strength (DTS) σ_{td} can be measured by:

$$\sigma_{td} = \frac{P}{A} \quad (1)$$

where the P is the applied peak load, and A is the cross-sectional area of the sample.

According to the ISRM (1978) and ASTM (2008), the Brazilian tensile strength (BTS) σ_{tb} is calculated by:

$$\sigma_{tb} = \frac{2P}{\pi DT} = 0.636 \frac{P}{DT} \quad (2)$$

where D represents the diameter of the disk, and T refers to the thickness at the center of the sample.

To date, compared to the direct tensile test, the Brazilian test consisting of the diametric compression of solid discs between flat or curved platens has been applied in lots of investigations. It owes its popularity to the ease of specimen preparation and the common experimental techniques required. However, a non-negligible difference between the DTS and BTS of rocks was reported by considerable researchers. Liu et al. (2014) found that the tensile strength of Beishan granite in the Brazilian test with simplified ISRM standard is 18% higher than that in the direct tensile test. By fitting the results of numerous existing literature, Perras and Diederichs (2014) proposed that tensile strength determined from direct and indirect methods is seldom equivalent, and the DTS is two-thirds of BTS. Wang et al. (2019) found an increment of 106% in the BTS of marble compared with its DTS. Fahimifar and Malekpour (2012) published their work on limestone specimens and proposed that the BTS is 1.11 times as large as the DTS. In particular, most of the previous research has focused on rocks in their natural state, and the comparative study on the DTS and BTS of water-saturated rock is rare. After all, the direct tensile tests of saturated rocks have only been conducted in a few specific cases (Hashiba and Fukui 2015; Zhu et al. 2022), let alone the comparative studies on tensile strength in the direct tensile test and the Brazilian test. To the best of our knowledge, this dilemma is mainly due to the controls of experimental procedure and sample preparation. Since the rock tensile strength is highly sensitive to its primary defect and experimental precision, measuring the DTS of saturated rocks under the premise of high homogeneity and consistent failure patterns is quite challenging.

Concerning the explanation of the difference between the DTS and the BTS of rock, Hoek (1964) and Perras and Diederichs (2014) believed that Brazilian tests overestimate the true tensile strength because of the external influence, such as the boundary conditions and stress distribution. Xie et al. (2005) suggested that the increase in the degree of tension results in easier energy release and

more rock strength reduction. In this line, Gorski et al. (2007) indicated that the combination of compressive and tensile stresses may be responsible for the great BTS. By a grain-based model with a universal discrete element code (UDEC), Qi et al. (2019) proposed that the greater shear stiffness of the grain boundary in the Lac du Bonnet granite may be the main factor controlling the difference between its DTS and BTS. Although several reasons (i.e., external conditions and tensile stress) have been proposed to describe the difference between DTS and BTS qualitatively, a substantial and quantifiable interpretation of this phenomenon is lacking. Another aspect to be noted is that the explanation of the difference between DTS and BTS of saturated rocks becomes complex because of the combination of water-weakening effects. Various water-weakening effects, e.g., friction weakening, pore water pressure, and stress corrosion, are often exerted at the same time, and detangling the contribution of one specific water-weakening effect is difficult (Kim and Changani 2016; Rabat et al. 2020b; Zhu et al. 2020). However, these water-weakening effects mentioned above are responsible for the tensile strength degradation of rocks. In this line, the combined effects of water saturation and loading conditions on rock tensile strength are not clear due to the limitation of quantitative analysis.

The deformation and fracture of rock is a process of the generation, nucleation, and propagation of cracks (Guo et al. 2022; Zheng et al. 2022). The localized strain energy emits outward as transient elastic waves during this process, which are referred to as acoustic emission (AE) activity. The AE technique has been proven to be a powerful method to investigate the micro-failure process of rock materials subjected to an external load (Aker et al. 2014; Lockner 1993; Manthei and Eisenblätter 2008). Two AE analysis methods, namely the AE parameter-based method and the AE waveform-based method, are extended according to the AE signal characteristics. The AE parameter-based method inferred from a series of AE parameters (i.e., AE count, AE event, and energy rate) is more widely used because of its convenience. The AE waveform-based analysis, however, requires high precision of the equipment and more working time. Aside from its shortcomings, the AE waveform-based analysis is worthwhile because the AE waveform signals released are believed to carry the intrinsic information of rock failure (Deng et al. 2018; Shiotani et al. 2001). In this context, many studies on AE waveform analysis have been conducted to understand the micro-failure process of various rock types (Huang et al. 2019; Li et al. 2017; Ohnaka and Mogi 1982; Zhang et al. 2018). Previous studies have targeted the characteristics of strength and deformation associated with failure using the dominant frequency and energy of AE waveform signals. Further, the dominant frequencies of AE waveforms are thought to be correlated to rock failure

patterns, such as micro-shear failure and micro-tensile failure, which may explain the strength variations under different loading conditions. However, the study on tensile strength variations explained by the AE waveform analysis of saturated rocks under direct and Brazilian tension is still in its infancy to date. The analysis of AE waveform characteristics may be a new way to evaluate the effects of water saturation and loading conditions on rock tensile strength.

The aforementioned points highlight that the effects of water saturation and loading conditions on rock tensile strength measured are important pending issues to be explored, and the AE waveform analysis is expected to be validly troubleshooting by evaluating the failure process of rock under tension. This paper is structured as follows: Sect. 2 provides an overview of the selected rock materials, as well as the experimental and analytical methods adopted. Section 3 presents the main experimental results, encompassing variations in tensile strength, statistical characteristics of AE waveforms, the correspondence between AE waveform types and micro-failure types, and the energy evolution of AE waveforms. Based on the experimental results, Sect. 4 engages in a discussion of three problems derived from the existing literature and the present study. Finally, Sect. 5 presents the conclusions drawn from the research.

2 Experimental Methodology

2.1 Rock Samples Preparation and Description

Two types of rock, including marble and granite, were used in this work. The marble block was taken from an open-pit mine located in Baoxing County (Sichuan Province, China), and the granite block was collected from the underground powerhouse of Dagangshan Hydropower Station in Dadu River Basin, located in Shimian County (Sichuan Province, China). To conduct the direct tensile test and Brazilian test following the ASTM methods, cylindrical core samples with two different size parameters, such as length (L) and the ratio of length to diameter (L/D), were drilled from each type of rock block. To be specific, cylindrical samples of two rocks were prepared with $\sim 2 L/D$ ratios (length: 100 mm, diameter: 50 mm) for direct tensile tests and $\sim 0.5 L/D$ ratios (length: 25 mm, diameter: 50 mm) for Brazilian tests. For simplicity, we refer to the samples prepared for the direct tensile test and Brazilian test as DT and BT samples in this study, respectively.

In addition, the chemical and mineralogical composition of the two rocks was determined using X-ray diffraction (XRD), X-ray fluorescence (XRF), and cross-polarized light (XPL). Some physical parameters (i.e., density and porosity) of samples were measured using traditional techniques.

XRD tests indicated that the marble rock used in this study is composed of calcite only, and 47% of quartz, 52% of bytownite, 0.5% of iron oxide, and 0.5% of aluminum phosphate were found in granite rock. In line with this, XRF analyses suggested that the chemical compound of marble is CaCO_3 (>99.9%), and those of granite are SiO_2 (68%), CaO (13%), Al_2O_3 (13%), Fe_2O_3 (1.5%) and AlPO_4 (2%). The thin-section images and chemical analysis of these two rocks are shown in Fig. 1. From the chemical analysis, we can infer that the marble rock is devoid of clay and siliceous minerals, and the granite rock is free of clay minerals; this is conducive to the analysis of water-weakening effects on rock tensile strength in the following study.

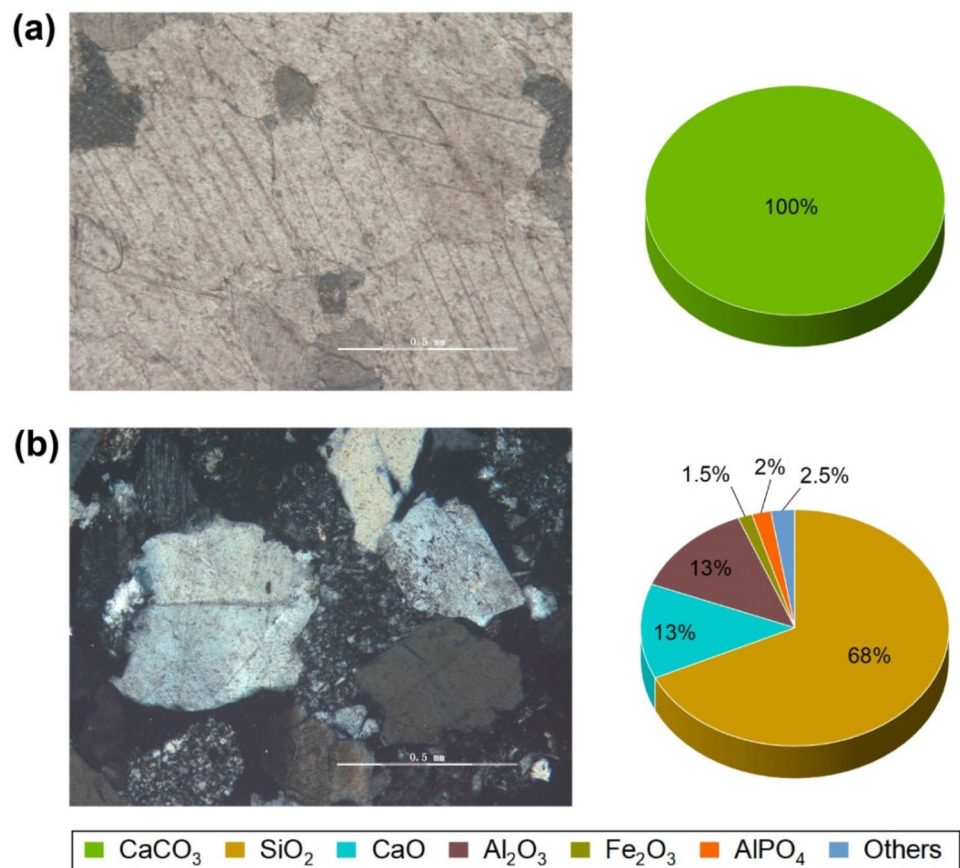
In total, 24 DT samples and 24 BT samples were heated in a 105°C oven for 48 h and then cooled down to room temperature. Half of the samples were stored in a dry container to prevent dampness and were ready for testing as dry samples. The remaining BT samples were soaked in purified water for 48 h inside a vacuum chamber with a pressure of -0.1 MPa over 48 h, followed by a 4 h standing period. The remaining DT samples were equipped with steel caps using JGN strong adhesive and left for 3–5 days. Afterward, samples with steel caps were all soaked in purified water under the same test procedure as the BT samples. To evaluate the

water absorption of different rock samples, we measured the water contents of marble and granite samples at various time intervals, as shown in Fig. 2. The correlation between the soaking time and the water content absorbed by the rocks was modeled using exponential fitting functions. It can be observed that constant water contents were reached for soaking time equal to or less than 24 h and 8 h for marble and granite, respectively. Hence, specimens immersed for 48 h in this study were believed to be in a fully saturated state. The physical and mechanical parameters are listed in Table 1.

2.2 Experimental Methods

The MTS 815 (Flex Test GT) rock mechanics machine with 1000 kN was applied to conduct the direct tensile test and Brazilian test (see Fig. 3). A real-time AE acquisition system (model: PCI-2) was used to capture the AE signals released during the entire loading process. The relative axial displacement was recorded by a linear variable differential transducer (LVDT) with a range of ± 2.5 mm. A total of eight micro30 sensors were symmetrically arranged on the surface of each sample. In the direct tensile test, as shown in Fig. 4, two rounds of AE sensors were installed near the top and bottom of the specimen,

Fig. 1 The thin-section images and chemical composition proportions of the tested rocks, **a** marble, **b** granite



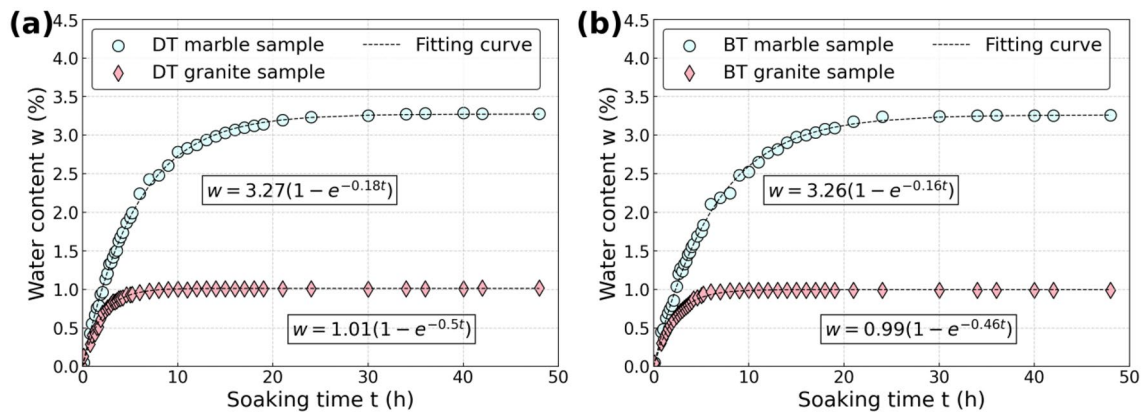


Fig. 2 The water content variation of two tested rocks with soaking time, a DT samples, b BT samples

Table 1 Summary of physical properties of two rocks studied

Rock type	ρ_{dry} (g/cm ³)	ρ_{sat} (g/cm ³)	P (%)	w (%)	V_{pd} (m/s)	V_{ps} (m/s)	σ_c (MPa)	E (GPa)	
Marble	$\chi(\pm\sigma)$	2.68 (± 0.014)	2.69 (± 0.008)	6.38 (± 0.033)	3.18 (± 0.013)	3024 (± 38)	3321 (± 35)	56.72	43.76
Granite	$\chi(\pm\sigma)$	2.78 (± 0.019)	2.80 (± 0.023)	1.72 (± 0.025)	0.97 (± 0.008)	5509 (± 66)	5722 (± 53)	120.05	40.43

χ : mean value, σ standard deviation, ρ_{dry} dry density, ρ_{sat} saturated density, P porosity, w water content, for saturated samples only, V_{pd} P-wave velocity of a dry sample, V_{ps} P-wave velocity of a saturated sample, σ_c uniaxial compressive strength of rock under natural conditions, E elastic modulus

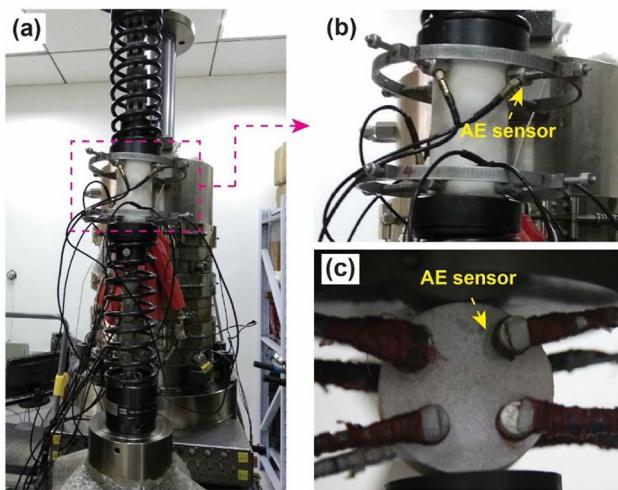


Fig. 3 Experimental setup used for a, b direct tension experiments, and c Brazilian experiments

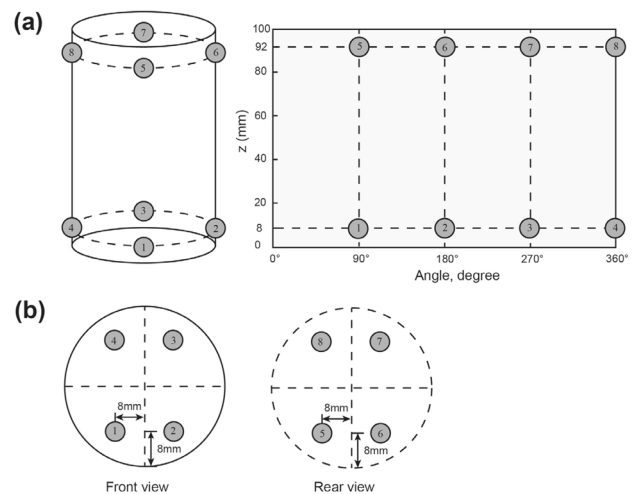


Fig. 4 The layout of AE sensors in a direct tension test, and b Brazilian test

and AE sensors with rectangle arrays were attached to the front and rear of the specimen in the Brazilian test. These micro30 sensors are highly sensitive and have a good frequency response to AE signals, making them beneficial to AE analysis. The pre-amplification and sampling rate of

AE monitoring were set as 40 dB and 1 MHz, respectively. A constant loading rate of 0.05 mm/min was applied during both the direct tensile test and the Brazilian test.

2.3 AE Waveform Data Processing

All AE waveform data was automatically recorded by the AE monitoring system and saved as numerous CSV files. The time element in the file name was adjusted to the front by Windows batch processing, which facilitates the identification of the AE waveform release time. With the aid of the MATLAB programming process, the Fast Fourier transformation (FFT) method was then employed to acquire the dominant frequencies of the AE waveform signals, as well as the corresponding loading time and amplitude. The dominant frequency, which is defined as the frequency corresponding to the maximum amplitude, could be determined by whose normalized amplitude is 1 in this study. For example, the dominant frequency shown in Fig. 5 is 98 kHz. The energy of AE signals was characterized by the square of their corresponding amplitude. As a result, all dominant

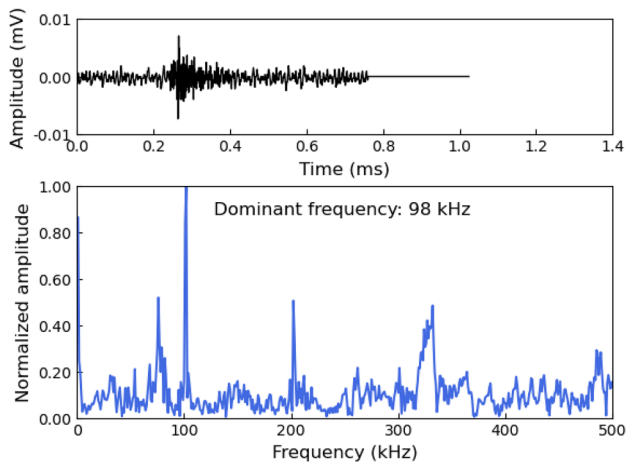


Fig. 5 The extraction process of the dominant frequency of an AE waveform

frequencies and their corresponding amplitude of the AE waveform signals could be efficiently recorded.

3 Results and Analysis

3.1 Rock Tensile Strength

The effect of water saturation on the direct tensile strength σ_{td} and the Brazilian tensile strength σ_{tb} of marble and granite is depicted in Fig. 6. The average σ_{td} values of dry and saturated marble are 2.58 and 1.86 MPa, whereas those of σ_{tb} values increase to 5.54 and 3.41 MPa, respectively. It can be found that the tensile strength in Brazilian tests is approximately 2.15 and 1.83 times that of direct tensile tests for dry and saturated marble, respectively. The average σ_{td} values of dry and saturated granite are 3.91 and 3.65 MPa, while those of σ_{tb} values increase to 7.17 and 6.52 MPa, respectively. In the same way as marble, multiple relationships between tensile strength from the Brazilian and direct tensile tests (i.e., 1.83 and 1.79) are found in dry and saturated granite. It means that the Brazilian loading leads to tensile strength enhancement, whether marble and granite are under dry or saturated conditions.

In addition, data showed that the σ_{td} and σ_{tb} diminished substantially in the marble studied due to water saturation. In particular, the percentage of reduction was 27.87% in σ_{td} and 38.48% in σ_{tb} for marble, respectively. Reductions of 6.64% and 9.04% are observed in σ_{td} and σ_{tb} , respectively, when granite undergoes saturation. It indicates that water saturation leads to a reduction in the tensile strength of both rocks under different loading conditions. In comparison, the weakening effect of water saturation on rock tensile strength is more pronounced in the Brazilian test than in the direct tensile test. Moreover, water saturation plays a more obvious role in the tensile strength reduction of marble than that of granite.

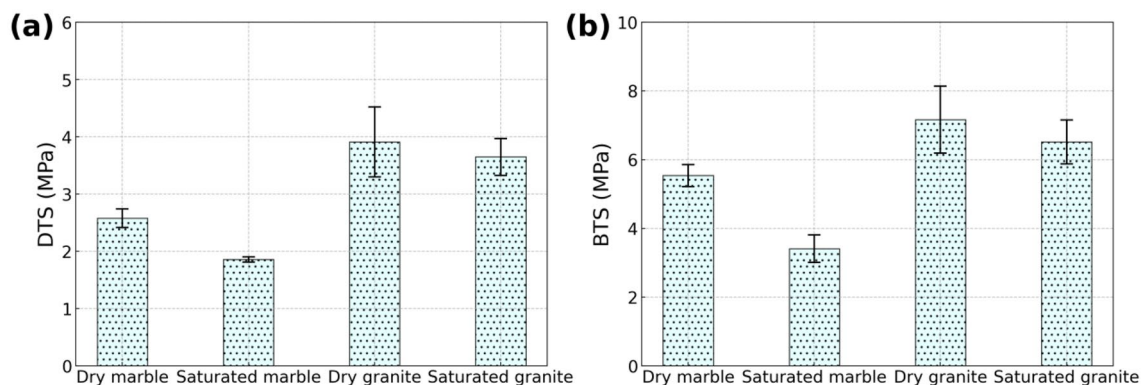


Fig. 6 The tensile strength of dry and saturated rocks under different loading conditions, **a** tensile strength in the direct tensile test, and **b** tensile strength in the Brazilian test

3.2 Statistical Analysis of AE Waveforms

To conduct statistical analysis, we divided the dominant frequencies of AE waveform signals into different bands. Concretely speaking, dominant frequencies less than 450 kHz were grouped into 45 bands with a constant interval of 10 kHz, and those greater than 450 kHz were classified into the 46th band. We then calculated the percentage of AE waveforms distributed in each dominant frequency band. The percentages of AE waveforms located in different dominant frequency bands of rocks are illustrated in Figs. 7 and 8.

An apparent feature of two concentrations in dominant frequency bands is observed, which is in line with several previous studies (Li et al. 2017; Zhang et al. 2022; Zhu et al. 2019). Further, we named these two concentrations of dominant frequency bands as high dominant frequency band (H-type band) and low dominant frequency band (L-type band), and AE waveforms distributed in high and low dominant frequency bands as H-type waveform and L-type waveform, respectively. The finding of two-peak frequency in this study enriches the research on AE spectrum analysis of rocks; this further confirms that the two-peak frequency is essential for rocks, irrespective of the soaking states and loading regime.

We selected the dominant frequency bands whose percentage is more than 1% and calculated the percentages

of H-type waveforms and L-type waveforms, as shown in Fig. 9. One can see that over 96% of the dominant frequencies are located in the H-type band and L-type band. This means the distribution of dominant frequencies is concentrated, and the classification of two categories is reasonable. Further, there is a mutually inhibiting relationship between the percentages of H-type waveforms and L-type waveforms because the sum of them is almost equal to 100%. We take the percentage of L-type waveforms as the representative to illustrate the effects of water saturation and loading conditions. On average, the percentages of L-type waveforms for dry marble in the direct tensile test and Brazilian test are approximately 91.42 and 38.55%, while those increase to 96.36 and 47.19%, respectively, when marble is saturated. The percentage of L-type waveforms for dry granite in the direct tensile test and Brazilian test account for approximately 69.91 and 24.29% on average, and those for saturated granite are 68.51 and 30.98%, respectively. It can be concluded that the water saturation and loading conditions have remarkable influences on the generation of AE waveforms located in different dominant frequency bands. Concretely, when rocks are saturated, the percentages of L-type AE waveforms considerably increase, except for granite in the direct tensile test (which remains almost unchanged). The percentage of H-type waveforms in AE signals of the Brazilian test

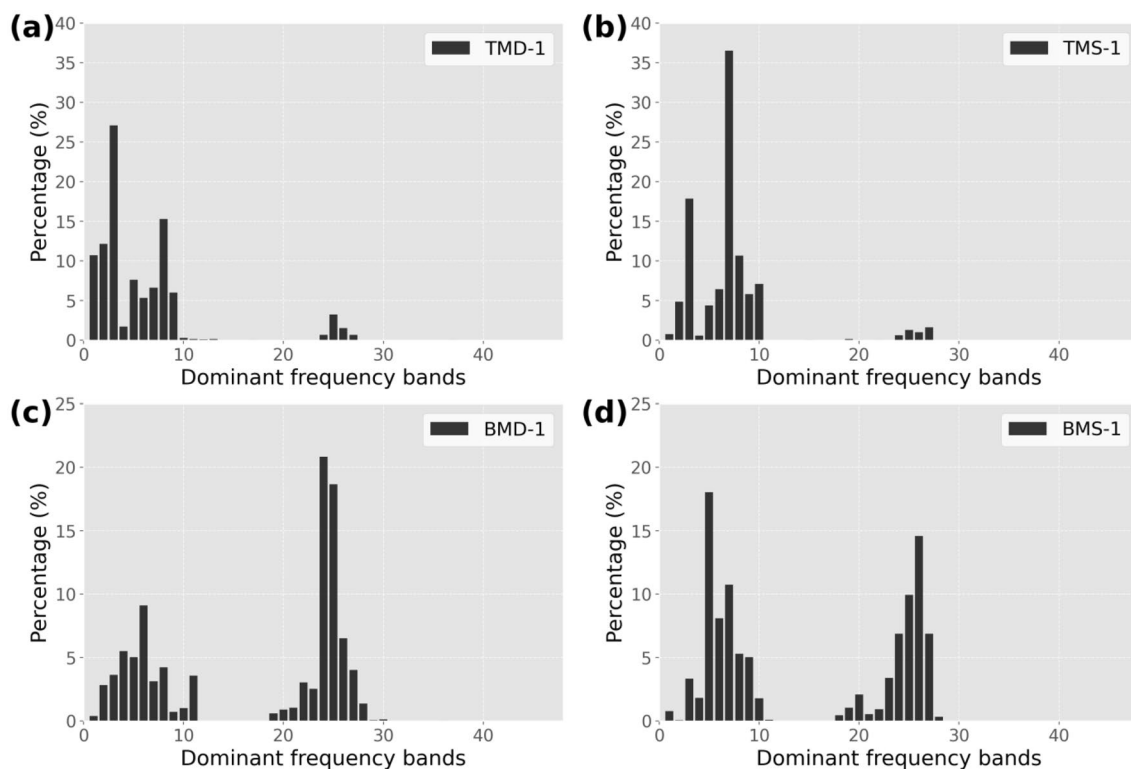


Fig. 7 The percentages of AE waveforms located in different dominant frequency bands of marble under different loading regimes

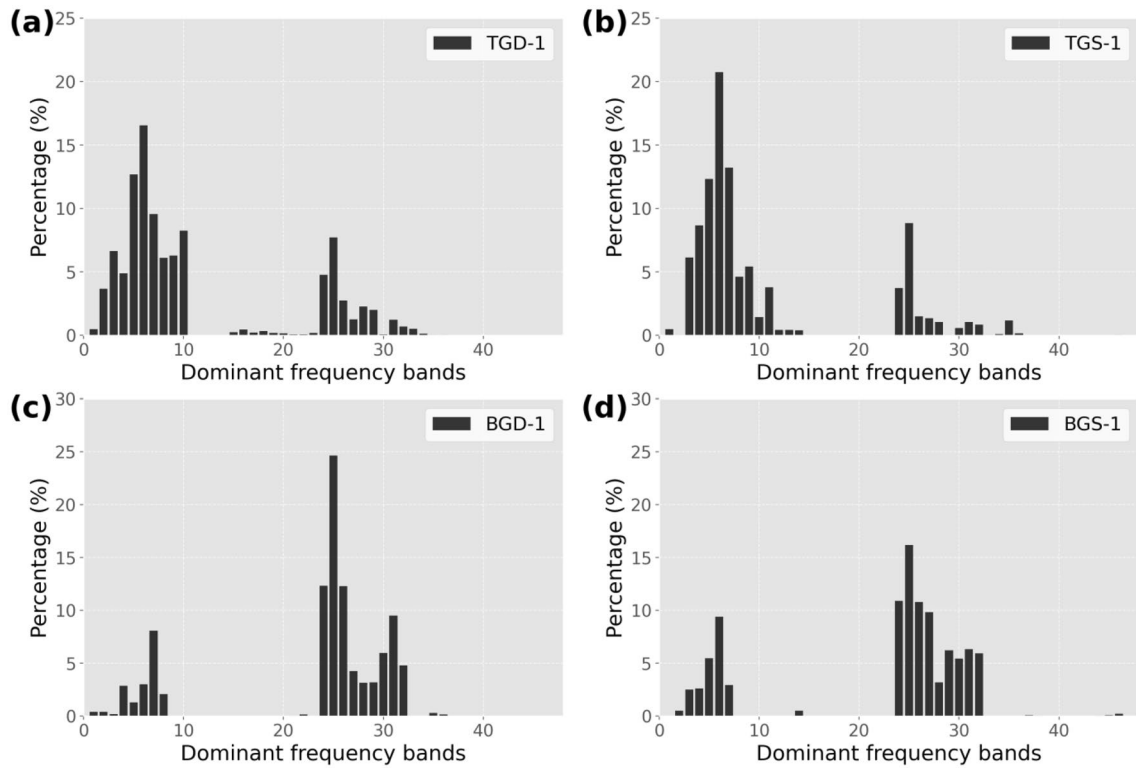


Fig. 8 The percentages of AE waveforms located in different dominant frequency bands of granite under different loading regimes

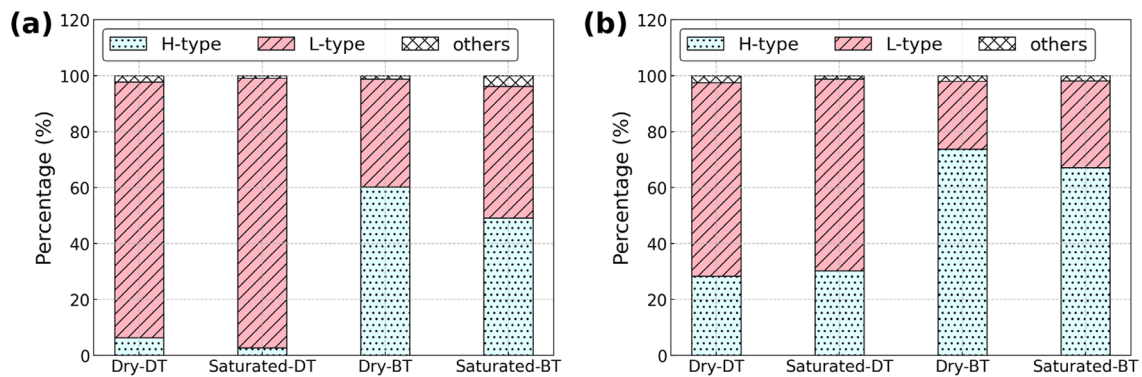


Fig. 9 The percentages of H-type waveforms and L-type waveforms of two rocks, **a** marble, and **b** granite. The data used in this plot is the average value of samples in the same group. The DT and BT in the

axial label indicate the direct tensile test and Brazilian test, respectively, and others mean AE waveforms distributed outside the high and low dominant frequency bands

is far greater than that of the direct tensile test, especially for the marble rock.

3.3 Dependence of Micro Failure on the Dominant Frequency of AE Waveform

The rock fracture is essentially a process of continuous accumulation and propagation of micro failures, which is the essential cause of rock strength. Herein, we used the

polarity method and AE parameters method to evaluate the AE source mechanism characterization; these two methods are commonly applied in the fracture mode classification of rock and concrete materials. The polarity method could conduct crack classification by the statistical result of signs of the first pulse amplitude of all hits in a single event. The polarity value of an event is obtained by Zang et al. (1998):

$$\text{pol} = \frac{1}{K} \sum_{i=1}^K \text{sign}(A_i) \quad (3)$$

In Eq. (3), A_i is the first pulse amplitude of the i th hit and K indicates the number of sensors used for an AE event. Classification is conducted within three selected ranges based on the polarity value, which corresponds to different types of micro failures. In particular, the tensile AE event is determined when $\text{pol} < -0.25$, the shear AE event is determined when $-0.25 < \text{pol} < +0.25$, and the compression AE event is evaluated when $\text{pol} > +0.25$. To simplify, the compression event is assumed to pertain to the shear event in this study.

A series of AE parameters are utilized to calculate two new parameters, i.e., the RA value and average frequency (AF) value, in the AE parameters method. According to numerous previous publications (Aggelis et al. 2011; Kordatos et al. 2012), the RA value and AF value are given by:

$$\text{RA} = \frac{T_r}{A_m} \quad (4)$$

$$\text{AF} = \frac{N}{T_d} \quad (5)$$

where N is the AE counts, T_d is the duration time, A_m is the maximum amplitude, and T_r is the rise time.

Shear and tensile cracks could be determined according to the relationship between the RA value and AF value. To be specific, a high RA value associated with a low AF value is caused by the propagation of cracks in the shear mode, and a lower RA value associated with a higher AF value is produced by the propagation of cracks in the tensile mode (Rodríguez and Celestino 2019; Wang et al. 2017). Taking marble specimens in the direct tensile test and Brazilian test as an example (see Fig. 10), the RA-AF values of TMD-1 are mostly distributed along the ordinate, which suggests

that tensile cracking is the dominant failure mode. The RA-AF values of BMD-1, however, are mostly exhibited along the abscissa, indicating the occurrence of abundant shear cracking. The percentages of micro-shear failure and micro-tensile failure of TMD-1 are 10.32 and 89.68%, and that of BMD-1 is 68.43 and 31.57%, respectively, when a transition line is determined. It should be noted that the ratio of AF value and RA value k , the slope of the transition line namely, is not a constant factor and varies under different experimental conditions and material types. Despite this uncertain condition of k , it was determined by empirical relationships in most previous literature (Farnam et al. 2015; Zhu et al. 2022). In this study, we set the k as 200:1 for all rock samples after several rounds of attempts and sort out their percentages of different crack types. A comparative study between the polarity method and the AE parameter method was then conducted. Further, we tried to explore the AE source mechanism and establish the correlation of crack types determined by these two methods mentioned above with the dominant frequency characteristic. Note that, crack and micro failure are not strictly distinguished in this study because crack types determined by the AE parameters method are described from a microscopic perspective.

In Fig. 11, it is evident that the results obtained using the polarity method and AE parameter method exhibit remarkable similarity across various scenarios, especially in the direct tensile test; no obvious dependence of water saturation on the consistent results of these two methods was observed. Data indicates that rock micro-tensile failures play a predominant role in the direct tensile test and their occurrence far surpasses that of micro-shear failures. The percentage of micro-shear failure for granite is higher compared to marble. This may be attributed to the differences in rock mineral composition and cementation type. In the Brazilian test, the micro-shear failures govern rock fracture generally, being more emphasized in granite. One important finding shows that there is correspondence between the AE

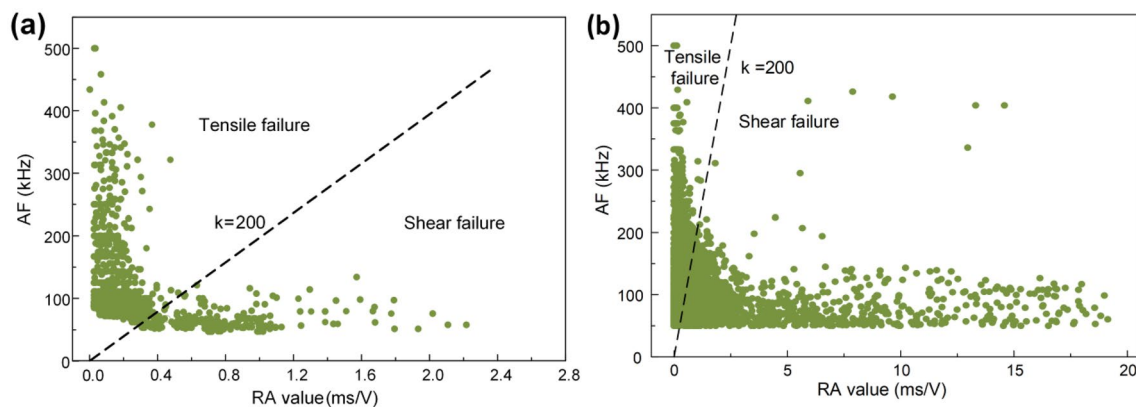


Fig. 10 The relationship between the RA value and AF of samples, **a** TMD-1, **b** BMD-1

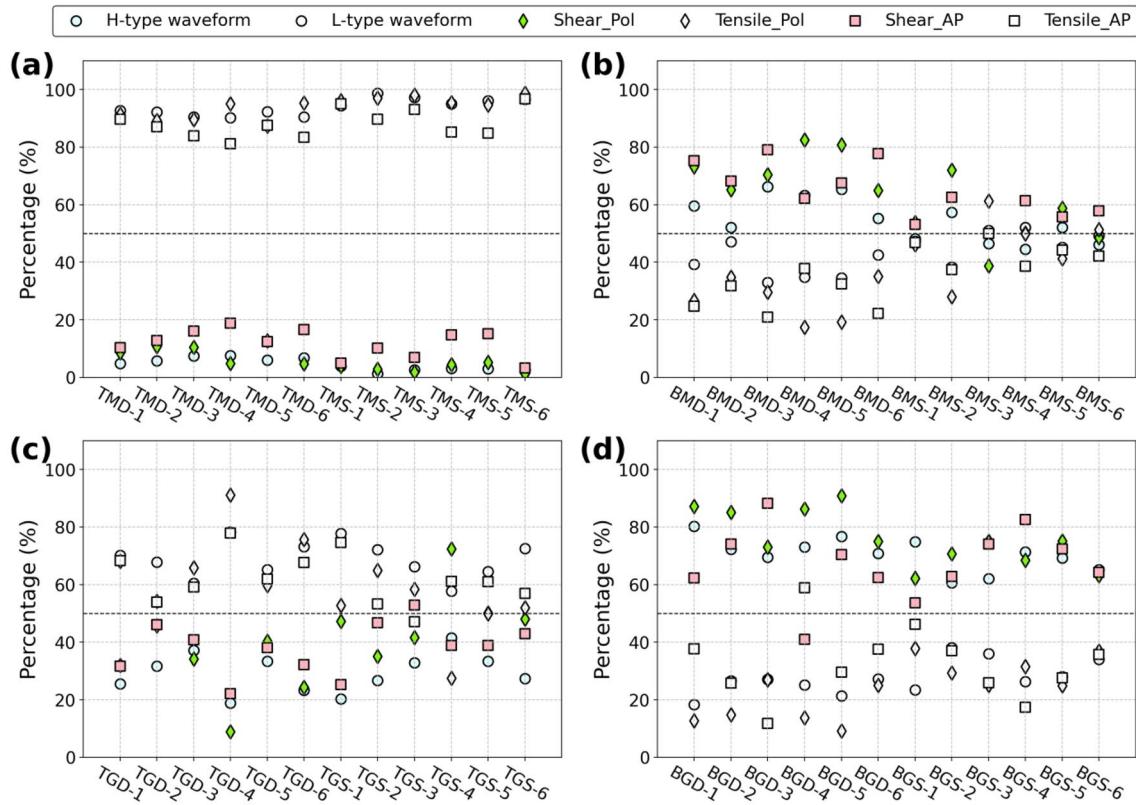


Fig. 11 The correlation of AE waveform types with failure types obtained by the polarity method and AE parameter method (the *_Pol* and *_AP* in the legend represent data values obtained by the polarity method and AE parameter method, respectively)

waveforms located in different dominant frequency bands and failure types, manifesting by their close value in percentage. Particularly, H-type waveforms typically correspond to the micro-shear failures and the L-type waveforms align well with micro-tensile failure. This finding is especially verified by the group of marble specimens in the direct tensile test, with the rather perfect consistency of data from dominant frequency analysis and these two crack classification methods. Overall, the correspondence between AE waveform

types and failure types is more obvious in the direct tensile test compared to the Brazilian test, with marble exhibiting a more pronounced association than granite.

3.4 AE Waveform Energy Evolution

The energy ratios of the H-type waveform and L-type waveform of the two rocks, i.e., P_{EH} and P_{EL} are depicted in Fig. 12. Results show that the sum of average energy ratios

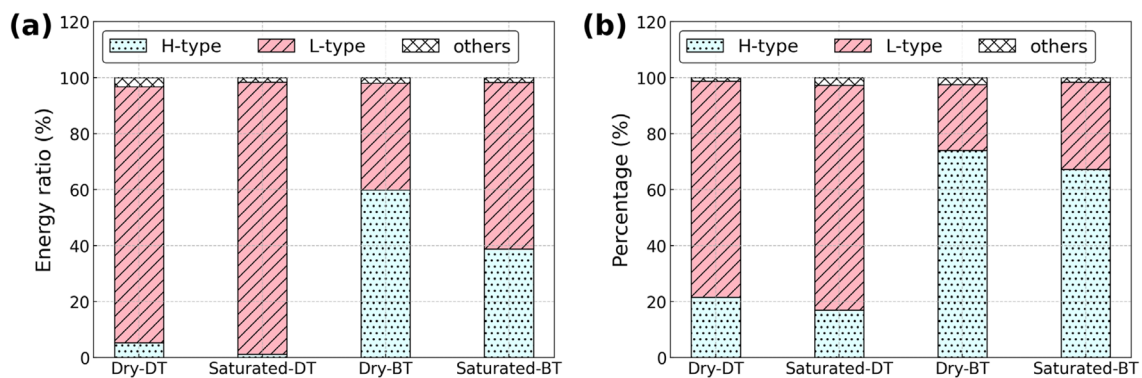


Fig. 12 The energy ratio of H-type waveforms and L-type waveforms of two rocks, **a** marble, and **b** granite

of the H-type waveform and L-type waveform for each group are all beyond 97%. This means the energy of AE waveforms that fell outside the two dominant frequency bands is very small and almost can be neglected during analysis. For marble in dry conditions, the average P_{EL} in the direct tensile test and Brazilian test are 91.39 and 38.12%, and these increase to 97.28 and 59.45 after saturation, respectively. A similar manner could be found in granite, that is, the average P_{EL} in the direct tensile test and Brazilian test for saturated granite are 80.30 and 31.11% compared to 77.20 and 23.53% for dry granite. These findings indicate that water saturation causes an increase in the energy ratio of the L-type waveform in both of these two test methods, along with a decreasing energy ratio of the H-type waveform. Moreover, it turns out that the increment or reduction in the energy ratio of the L-type or H-type waveform in the Brazilian test is greater than that in the direct tensile test, indicating a more obvious water saturation effect on the energy of rock failures in the Brazilian test.

4 Discussion

We documented the tensile strength of dry and saturated rocks under different loading conditions, as well as the dominant frequency characteristics (i.e., amount percentage and energy ratio) of AE waveforms. In this scene, we would like to discuss the following points: what causes the difference in rock tensile strength in the direct tensile test and the Brazilian test? Since the L-type waveform corresponds to micro-tensile failure, is it correlative with the rock tensile strength variation? What is the interpretation of water weakening effects on rock tensile strength under different loading conditions?

4.1 Difference Between Tensile Strength in the Direct Tensile Test and the Brazilian Test

The difference between rock tensile strength measured by the direct tensile test and the Brazilian test has been recognized. By fitting the experimental results from some existing literature (Andreev 1991a, b; Coviello et al. 2005; Graue et al. 2011; Klanphumeesri 2010; Mishra and Basu 2012; Perras and Diederichs 2014; Perras et al. 2013; Qi et al. 2019; Rabat et al. 2023; Ramana and Sarma 1987) and ours, we found that the ratios of BTS and DTS, χ namely, in this study were distributed in a range that matches other results (see Fig. 13). An interesting finding is that the existence of water seems to diminish the difference in the tensile strength between these two methods, manifesting in the smaller χ of marble and granite under saturated conditions (i.e., 1.83 and 1.79) compared to that under dry conditions (i.e., 2.15 and 1.83).

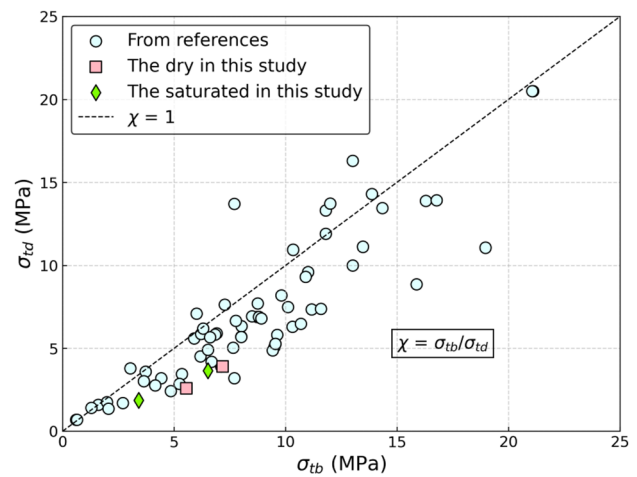


Fig. 13 Correlation between the Brazilian tensile strength and the direct tensile strength in marble and granite and comparison with other rock types published in the scientific literature

When rock is subject to direct tensile loading, micro-tensile failures dominate the rock fracture process, accompanied by a few micro-shear failures. In general, the micro-shear failures generated in the direct tensile test are considered as the interaction between mineral particles, e.g., friction caused by grain slip. Hence, the microstructure of rock affects the generation of micro-shear failures, that is, the more complex the microstructure of rock is, the more likely the micro-shear failures occur. The marble used in this study is more homogeneous than granite due to its single mineral composition, and few micro-shear failures thus occur. Since the H-type waveforms are caused by micro-shear failures analyzed in Sect. 3.3, as would be expected, the H-type waveforms released from marble are far less than that of granite in both two test methods. The loads experienced by the rock specimen during the Brazilian test are intricate. On one hand, the compressive load acting on the radial direction of the specimen would cause numerous micro-shear failures due to the close relationship between compression and shear failure. On the other hand, the compressive load makes the rock specimen undergo horizontal deformation and tensile stress generated, which is responsible for the generation of considerable micro-tensile failures. As a result, both H-type and L-type waveforms of rock are abundant in the Brazilian test, and sometimes the former is more pronounced.

It is generally believed that direct tensile testing yields the true tensile strength of rock, whereas Brazilian tensile testing makes an over-measurement. In this study, the Brazilian test produces a higher percentage of H-type waveforms, and higher tensile strength was measured; this means that more micro-shear failures occurred in the Brazilian test compared to the direct tensile test. As we know, the ability of a brittle rock to compress is much greater than that to

stretch (Goodman 1989; Wu et al. 2018). Xie et al. (2005) and Wang et al. (2019) have demonstrated that micro-shear failure plays a synergistic role in rock fracture, and its high percentage indicates a high blocking effect on energy release and great critical stress. This is why saturated rocks, which release more L-type waveforms (corresponding to micro-tensile failures), have lower strength than dry rocks. As shown in Fig. 14, the failure of rock specimens under direct tension is mainly the result of overcoming the cohesion between the mineral particles and the friction generated. Taking the lower part of the specimen as an example, three forces, including the tensile force T , the cohesion force F_{cd} , and the friction force f_1 , is activated. Among them, the T is balanced by the resultant force of F_{cd} and f_1 . As analyzed, the f_1 generated on the potential failure surface, which is caused by the tendency or occurrence of crystal particles to slip, is expected to be a considerable component of rock specimen tension capacity. Similar to the manner of the specimen in the direct tensile test, the friction that occurred on the potential failure surface in the Brazilian test could be one of the reasons for the Brazilian tensile strength. It should be noted that the failures generated by overcoming friction are most likely to be characterized by micro-shear failures. In this connection, the fact that the Brazilian tensile strength is greater than the direct tensile strength can be attributed to the generation of abundant micro-shear failures induced by compressive load and friction. In a word, the friction generated on the potential failure surfaces is a non-negligible component of the tensile strength, and the micro-shear failures, which are manifested by the H-type waveforms, are the immediate cause of the difference between the direct tensile strength and the Brazilian tensile strength. Specifically,

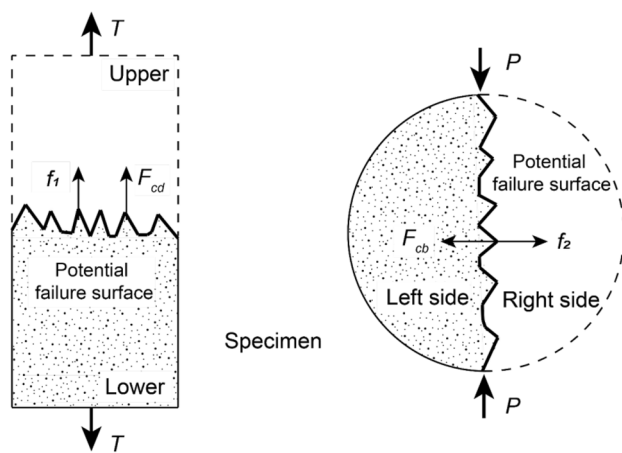


Fig. 14 Schematic diagram of forces acting on rock specimen in the direct tensile test and the Brazilian test. f_1 , F_{cd} , and T are the frictional force, cohesion force, and applied tensile load in the direct tensile test, respectively. f_2 , F_{cb} , and P are the frictional force, cohesion force, and applied compressive load in the Brazilian test, respectively

the more the micro-shear failures are, the higher the tensile strength is.

4.2 Correlation of Tensile Strength with the Energy Ratio of L-Type Waveform

From a microscopic perspective, the previous findings indicate that the rock types and external conditions affect the statistical characteristics of different types of micro failures, which causes the rock tensile strength to vary. It is important to note that the tensile strength measured in the direct and Brazilian loading tests in this study does not represent the true tensile strength, as the percentage of micro-tensile failure is not equal to 100%. In fact, among the existing experimental conditions that are used to measure the rock tensile strength, pure tensile loading cannot be currently implemented. Herein, we defined an “ideal” tensile strength according to the physical meaning of rock tensile strength; it corresponds to the condition that the micro-tensile failures account for 100%. Given the corresponding relationship between micro-failure and AE waveform types, we selected the L-type waveforms as a representative indicator to evaluate the “ideal” tensile strength of rock.

The AE waveform signals are generated as a result of rock micro failures, which occur due to the release of localized strain energy. Compared to the quantity of AE waveform signals, its energy can better characterize the intensity of rock micro failure. Therefore, we explored the correlation between rock tensile strength and the energy ratio of L-type waveforms to predict the “ideal” tensile strength. As shown in Fig. 15, the direct tensile strength is negatively correlated with the energy ratio of L-type waveforms. We determined the “ideal” tensile strength by identifying the intersection point of a linear fitting curve, where the energy ratio of L-type waveforms accounts for 100%. Moreover, the higher Brazilian tensile strength results from the fewer L-type waveforms according to the findings mentioned above. This indicates a direct correlation between the Brazilian tensile strength and the L-type waveform. Based on this, we integrated the data from the Brazilian test to enhance the prediction of the “ideal” tensile strength. In other words, we employed two linear fitting curves, each determined by different sets of original data (i.e., data solely from the direct tensile test and data combined from the direct tensile test and the Brazilian test) to predict the “ideal” tensile strength using their intersection points. From Fig. 15, one can see that the tensile strength of both two test methods versus the energy ratio of the L-type waveform follows a linear law relationship. The correspondence between the tensile strength of rocks in dry conditions and the energy ratio of the L-type waveform is stronger compared to rocks in saturated conditions, exhibiting a higher correlation coefficient.

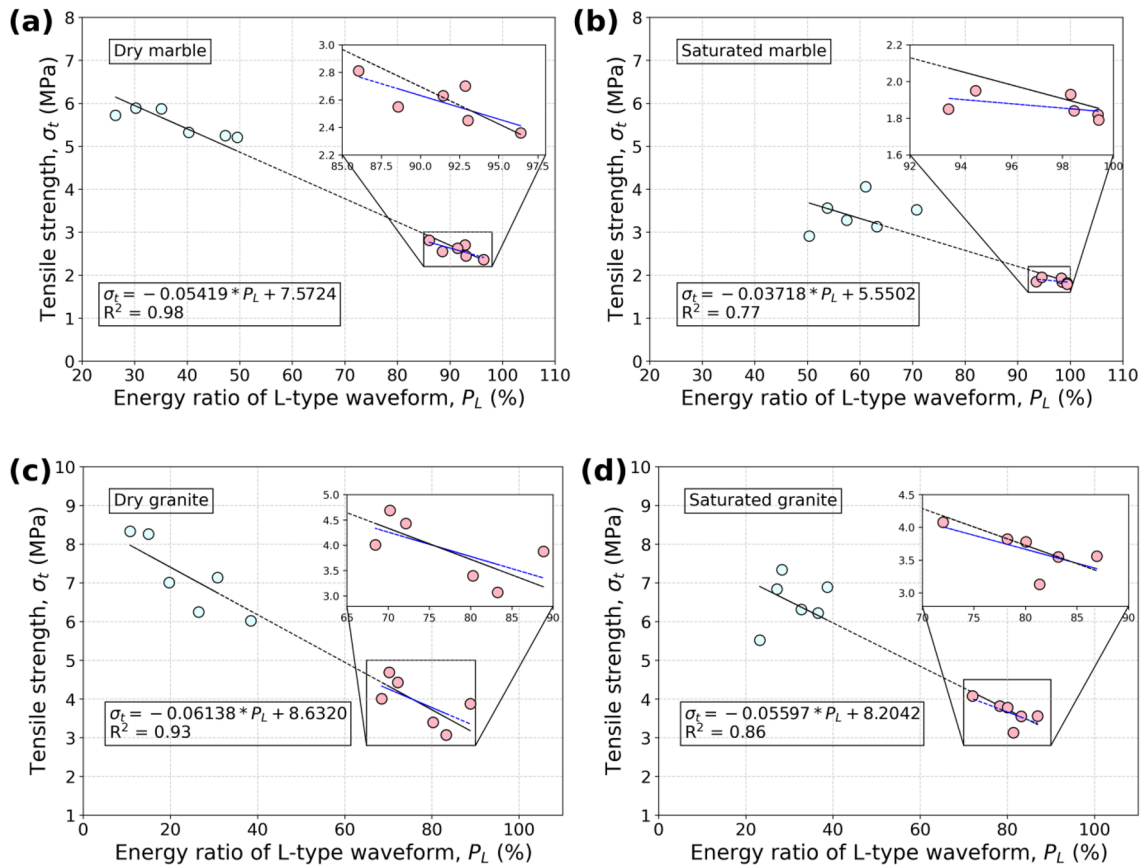


Fig. 15 The correlation of tensile strength with the energy ratio of L-type waveforms (the black dotted line is the linear fitting curve for samples in the direct tensile test and Brazilian test, and the blue dot-

ted line is the linear fitting curve for the samples in the direct tensile test. For interpretation of the references to color in this figure legend, the reader is referred to the web version of this article)

The results of predicting the “ideal” tensile strength using these two fitting methods are shown in Fig. 16. The fitting method that combines both DTS and BTS data was referred to as “Fitting method 1”, while the fitting method that solely relies on DTS data was denoted as “Fitting method 2”. The “ideal” tensile strength of dry marble, saturated marble, dry granite, and saturated granite by Fitting method 1 is 2.15, 1.83, 2.49, and 2.60 MPa compared to average values of 2.58, 1.86, 3.91, and 3.65 MPa obtained from the direct tensile test. This suggests that the “ideal” tensile strength obtained by fitting method 1 is lower than the average value. Similar conditions could also be found in the results by Fitting method 2, indicating that the high energy ratio of the L-type waveform (i.e., 100%) is the reason for the reduction in “ideal” tensile strength. This further supports the close relationship between the characteristics of the L-type waveform (amount and energy ratio) and rock tensile strength, given the rock’s weak ability to stretch.

The difference between the tensile strength measured under experimental conditions and the estimated “ideal” tensile strength is smaller for marble than for granite. Although the fitting methods based on spectrum analysis and dominant

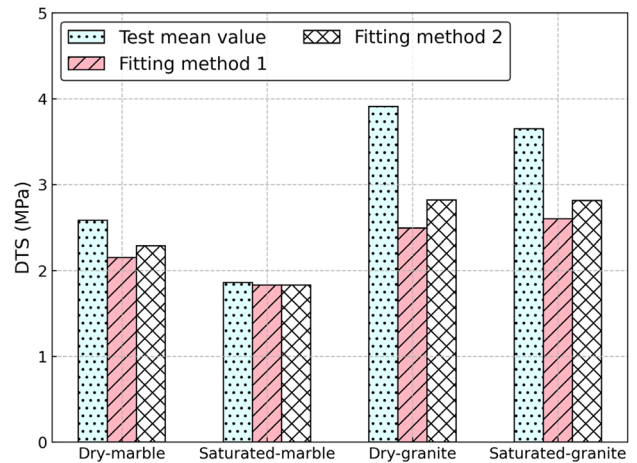


Fig. 16 The direct tensile strength of rocks determined by different methods (fitting method 1 in the figure legend indicates the results from the fitting curve by the tensile strength in the direct tensile test and the Brazilian test shown in Fig. 15, and the Fitting method 2 indicates the results from the fitting curve by the tensile strength in the direct tensile test shown in Fig. 15)

frequency statistics are time-consuming, they provide more accurate tensile strength predictions and can be used as an alternative in early rock engineering design. In general, Fitting method 1 tends to yield lower “ideal” tensile strength compared to Fitting method 2 and thus less aligned with the average value from the direct tensile test. On one hand, the considerable amount of H-type waveforms induced by the loading condition in the Brazilian test may impede the fitting accuracy in Fitting method 1 to some extent. On the other hand, the additional data points from the Brazilian tests make the fitting results in Fitting method 1 more convincing. In this study, we attempted to incorporate the Brazilian tensile strength in Fitting method 1 and successfully predicted the “ideal” tensile strength of marble and granite with acceptable errors. Nevertheless, further studies are required to assess the accuracy of these two fitting methods for a broader range of rock types, as the data samples in this work were limited.

4.3 Water Saturation Effects on Rock Tensile Strength Under Different Loading Conditions

The intrinsic mechanisms that underlie the reduction in tensile strength of rocks due to water are multifaceted and intricate. In particular, the following reasons are proposed in the existing literature: clay mineral swelling, pore water pressure, friction weakening, and stress corrosion (Brantut et al. 2014; Cai et al. 2022; Erguler and Ulusay 2009; Rabat et al. 2021). It is worth noting that, the exertion of the multiple potential mechanisms depends on the rock types and experimental conditions. Concerning these possible reasons, the clay mineral swelling and stress corrosion occur in the rocks containing clay and siliceous minerals, respectively. The effects of pore water pressure and friction weakening are largely correlated to the porosity and solubility of rocks.

Moreover, the pore water pressure effect is generally considered negligible under a pure tensile loading regime. It is, therefore, reasonable to posit that the friction weakening effect could be the primary weakening mechanism responsible for the reduction in strength of saturated marble, given its mineral composition (calcite only). Due to the abundant siliceous minerals in saturated granite, the water-induced reduction in its strength is possibly attributed to the combined effects of friction-weakening and stress corrosion. Subsequently, we would like to discuss separately the water-weakening effects responsible for the tensile strength reduction of marble and granite under different loading conditions.

In Sect. 4.1, we elucidated that the friction generated on the potential failure surface is a contributing factor to the tensile strength of the rock. When rocks are saturated, the friction weakening induced by water arises, leading to a reduction in tensile strength. As shown in Fig. 17, a typical scanning electron microscope (SEM) image of dry marble rock in a direct tensile test reveals the presence of multiple smooth failure surfaces, which signify transgranular fractures characterized by violent rupture patterns. Conversely, the SEM image of saturated rock showcases rough convex surfaces adorned with flat blunt angulars, indicating the weakening friction induced by water. The friction-weakening effect in rocks is typically attributed to chemical and physical interactions, such as the ion exchange and solution, and adsorbed water films on mineral surfaces (Cai et al. 2019; Van 1976; Zhou et al. 2018). Although the dissolution of calcite minerals is very limited in current scenarios due to vacuum saturation and the short test duration, the presence of lubricating water films on mineral surfaces can largely reduce the friction between mineral particles, thereby leading to tensile strength degradation. This is strongly supported by the proportion reductions in the amount and energy of the H-type waveforms (micro-shear

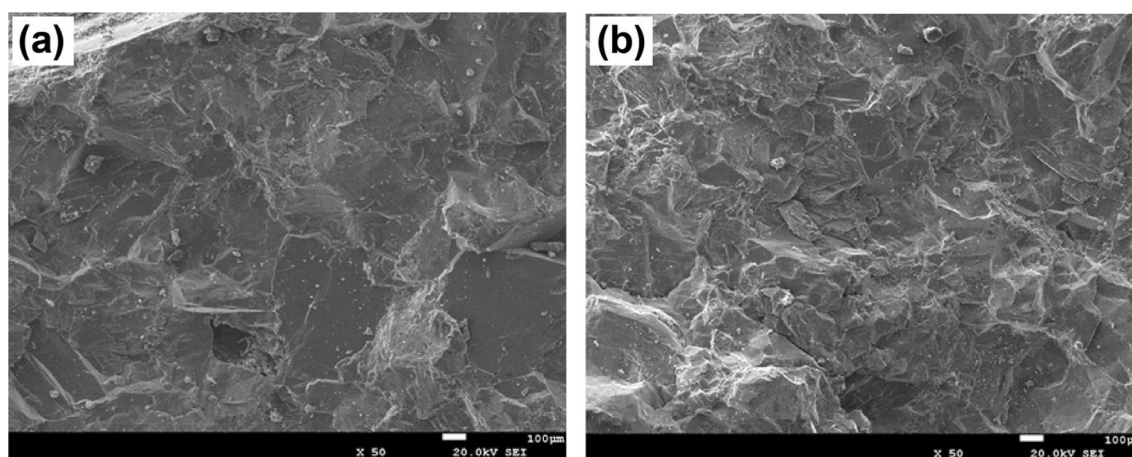


Fig. 17 The SEM images of marble samples in the direct tensile tests, **a** dry marble sample, **b** saturated marble sample

failures) which are closely related to friction weakening. For example, the proportion reductions in amount and energy of H-type waveforms for saturated marble in the direct tensile are 3.64 and 3.55%, and those in the Brazilian test are 11.16 and 24.55%, respectively. Due to the complementary relationship between H-type and L-type waveforms in proportion, the amount and energy of L-type waveforms considerably increase. Moreover, it should be recalled that the tensile strength reductions of saturated marble in the direct tensile test and the Brazilian test are 27.87 and 38.48%, respectively. It means that the water-weakening effects on tensile strength are more obvious under Brazilian loading than direct tensile loading. A reasonable explanation of this difference is that the friction-weakening effect caused by lubricating water films in the Brazilian test is more prominent under the condition of widespread friction implied by the abundant micro-shear failures. In a word, the friction weakening effect induced by water films is responsible for the reduction in tensile strength under both direct tensile loading and Brazilian loading, and the widespread friction condition in the Brazilian test facilitates the occurrence of friction weakening, as evidenced by the substantial reduction in Brazilian tensile strength.

Saturated granite is likely to suffer from two main water-weakening effects, including friction weakening and stress corrosion. Results showed reductions of 6.64 and 9.04% in the direct tensile strength and Brazilian tensile strength when granite is saturated. However, the proportion of H-type waveforms in amount exhibited an increment of 1.99% in the direct tensile test, and that emphasized a reduction of 6.58% in the Brazilian test. Moreover, the proportion reductions of H-type waveforms in energy are 3.36 and 6.10% in the direct tensile and Brazilian tests, respectively. This is similar to the condition of saturated marble in some aspects, such as greater reduction in tensile strength observed in the Brazilian test, and greater reductions in the amount and energy of H-type waveform in the Brazilian test. Therefore, we can rationally speculate that the friction-weakening effect plays a considerable role in the tensile strength degradation of saturated granite, particularly in the Brazilian test. In addition to the friction weakening effect, the potential stress corrosion in saturated granite is actually a process of chemical hydrolysis. The stress corrosion theory suggests that the crack propagation velocity increases when water vapor condensates in the crack tips of rocks, acting as a corrosive agent. That is, the replacement of silica-oxygen bonds by weaker hydrogen bonds caused by water reduces the stress required for rock failure, which would facilitate the initiation and propagation of cracks (Oldecop and Alonso 2007). It should be noted that the process of stress corrosion is slow and only valid when water can diffuse into newly created crack tips (Atkinson and Meredith 1981). The experimental conditions in this study, i.e., test duration over 10 min and

tensile stress distribution, could lead to the occurrence of stress corrosion. However, the porosity of granite (1.72%, see Table 1) is too low to allow the diffusion of too much water, even though the saturation state is reached. This is why the loss in tensile strength for saturated granite is quite lower relative to saturated marble. Compared to the friction-weakening effect caused by lubricating water films, stress corrosion occurs under more severe conditions. Hence, both friction weakening effect and stress corrosion are considered as the reasons for the reduction in tensile strength of saturated granite, but the former is more pronounced.

5 Conclusions

Based on the experimental work and AE analyses conducted in the present article, several essential points can be highlighted:

- (1) Water saturation causes substantial reductions in the tensile strength of marble and granite under different loading conditions. In both dry and saturated conditions, the tensile strength of rocks in the Brazilian test is greater than that in the direct tensile test. This disparity is attributed to the occurrence of more micro-shear failures during Brazilian loading compared to direct tensile loading.
- (2) Brazilian loading leads to an increment in the percentage of H-type waveforms, while water saturation typically increases the percentage of L-type waveforms. The results of crack classification methods (such as the polarity method and the AE parameters method) demonstrate a correspondence between the AE waveform types and micro-failure types. H-type waveforms are produced by micro-shear failures, whereas L-type waveforms are caused by micro-tensile failures.
- (3) Water saturation induces variations in the energy ratio of different AE waveform types, particularly an increase in the energy ratio of L-type waveforms. The energy ratio of L-type waveforms shows a close correlation with tensile strength and can be used to predict the “ideal” tensile strength. Tensile strength determined through different fitting methods is lower than the experimental direct tensile strength but within acceptable error ranges.
- (4) The friction-weakening effect induced by lubricating water films is responsible for the tensile strength reduction of saturated marble and saturated granite under different loading conditions. The greater tensile strength reduction in the Brazilian test is attributed to its pronounced friction weakening effect due to the widespread friction condition during loading. Stress

corrosion could be the secondary cause of the tensile strength reduction of saturated granite.

Acknowledgements This research was supported by the foundation of the Key Laboratory of Deep Earth Science and Engineering (Sichuan University), Ministry of Education (Grant No. DUSEYU202304), National Natural Sciences Foundation of China (Grant No. U21A2008 and U19A2098), CAS Light of West China Program (Grant No. 2021160160) and Sichuan Science and Technology Program (Grant No. 2023NSFSC0786). The authors thank the anonymous reviewers and the editor for comments that significantly improved the manuscript.

Data Availability The data that support the findings of this study are available from the corresponding author upon reasonable request.

Declarations

Conflict of interest The authors declare that they have no known competing financial interests or personal relationships that could have appeared to influence the work reported in this paper.

References

- Aggelis D, Kordatos E, Matikas T (2011) Acoustic emission for fatigue damage characterization in metal plates. *Mech Res Commun* 38(2):106–110
- Aker E, Kühn D, Vavryčuk V, Soldal M, Oye V (2014) Experimental investigation of acoustic emissions and their moment tensors in rock during failure. *Int J Rock Mech Min Sci* 70:286–295
- Andreev G (1991a) A review of the Brazilian test for rock tensile strength determination. Part I: calculation formula. *Min Sci Technol* 13(3):445–456
- Andreev G (1991b) A review of the Brazilian test for rock tensile strength determination. Part II: contact conditions. *Min Sci Technol* 13(3):457–465
- ASTM (2008) D3967-08: standard test method for splitting tensile strength of intact rock core specimens. ASTM International, West Conshohocken
- Atkinson BK, Meredith PG (1981) Stress corrosion cracking of quartz: a note on the influence of chemical environment. *Tectonophysics* 77(1–2):T1–T11
- Bajni G, Apuani T, Beretta GP (2019) Hydro-geotechnical modelling of subsidence in the Como urban area. *Eng Geol* 257:105144
- Brantut N, Heap MJ, Baud P, Meredith PG (2014) Mechanisms of time-dependent deformation in porous limestone. *J Geophys Res Solid Earth* 119(7):5444–5463
- Cai X, Zhou Z, Liu K, Du X, Zang H (2019) Water-weakening effects on the mechanical behavior of different rock types: phenomena and mechanisms. *Appl Sci* 9(20):4450
- Cai X, Cheng C, Zhao Y, Zhou Z, Wang S (2022) The role of water content in rate dependence of tensile strength of a fine-grained sandstone. *Arch Civ Mech Eng* 22(1):1–16
- Coviello A, Lagioia R, Nova R (2005) On the measurement of the tensile strength of soft rocks. *Rock Mech Rock Eng* 38(4):251–273
- Dang W, Wu W, Konietzky H, Qian J (2019) Effect of shear-induced aperture evolution on fluid flow in rock fractures. *Comput Geotech* 114:103152
- Deng J, Li L, Chen F, Yu J, Liu J (2018) Twin-peak frequencies of acoustic emission due to the fracture of marble and their possible mechanism. *Adv Eng Sci* 50(5):12–17
- Erguler ZA, Ulusay R (2009) Water-induced variations in mechanical properties of clay-bearing rocks. *Int J Rock Mech Min Sci* 46(2):355–370
- Fahimifar A, Malekpour M (2012) Experimental and numerical analysis of indirect and direct tensile strength using fracture mechanics concepts. *Bull Eng Geol Environ* 71(2):269–283
- Farnam Y, Geiker MR, Bentz D, Weiss J (2015) Acoustic emission waveform characterization of crack origin and mode in fractured and ASR damaged concrete. *Cement Concr Compos* 60:135–145
- Goodman R (1989) Introduction to rock mechanics, 2nd edn. Wiley, New York
- Gorski B, Conlon B, Ljunggren B (2007) Forsmark site investigation: determination of the direct and indirect tensile strength on cores from borehole KFM01D. *Svensk kärnbränslehantering (SKB)*
- Graue B, Siegesmund S, Middendorf B (2011) Quality assessment of replacement stones for the Cologne Cathedral: mineralogical and petrophysical requirements. *Environ Earth Sci* 63(7):1799–1822
- Guo J, Zheng J, Lü Q, Deng J (2022) Estimation of fracture size and azimuth in the universal elliptical disc model based on trace information. *J Rock Mech Geotech Eng* 15(6):1391–1405
- Hashiba K, Fukui K (2015) Effect of water on the deformation and failure of rock in uniaxial tension. *Rock Mech Rock Eng* 48(5):1751–1761
- Hoek E (1964) Fracture of anisotropic rock. *J S Afr Inst Min Metall* 64(10):501–518
- Huang Y, Deng J, Zhu J (2019) An experimental investigation of moisture-induced softening mechanism of marble based on quantitative analysis of acoustic emission waveforms. *Appl Sci Basel* 9(3):446
- ISRM (1978) Suggested methods for determining tensile strength of rock materials. *Int J Rock Mech Min Sci Geomech Abstr* 15(1):99–103
- Jiang Q, Cui J, Feng X, Jiang Y (2014) Application of computerized tomographic scanning to the study of water-induced weakening of mudstone. *Bull Eng Geol Environ* 73(4):1293–1301
- Kim E, Changani H (2016) Effect of water saturation and loading rate on the mechanical properties of Red and Buff sandstones. *Int J Rock Mech Min Sci* 88:23–28
- Klanphumesri S (2010) Direct tension testing of rock specimens. Suranaree University of Technology
- Kordatos E, Aggelis D, Matikas T (2012) Monitoring mechanical damage in structural materials using complimentary NDE techniques based on thermography and acoustic emission. *Compos B Eng* 43(6):2676–2686
- Li L, Deng J, Zheng L, Liu J (2017) Dominant frequency characteristics of acoustic emissions in white marble during direct tensile tests. *Rock Mech Rock Eng* 50(5):1337–1346
- Liu J, Chen L, Wang C, Man K, Wang L, Wang J, Su R (2014) Characterizing the mechanical tensile behavior of Beishan granite with different experimental methods. *Int J Rock Mech Min Sci* 69(3):50–58
- Lockner D (1993) The role of acoustic emission in the study of rock fracture. *Int J Rock Mech Min Sci Geomech Abstr* 30(7):883–899
- Ma D, Duan H, Li X, Li Z, Zhou Z, Li T (2019) Effects of seepage-induced erosion on nonlinear hydraulic properties of broken red sandstones. *Tunn Undergr Space Technol* 91:102993
- Manthei G, Eisenblätter J (2008) Acoustic emission in study of rock stability. *Acoustic emission testing*. Springer, Berlin, pp 239–310
- Mishra D, Basu A (2012) Use of the block punch test to predict the compressive and tensile strengths of rocks. *Int J Rock Mech Min Sci* 51:119–127
- Ohnaka M, Mogi K (1982) Frequency characteristics of acoustic emission in rocks under uniaxial compression and its relation to the fracturing process to failure. *J Geophys Res Solid Earth* 87(B5):3873–3884
- Oldecop LA, Alonso E (2007) Theoretical investigation of the time-dependent behaviour of rockfill. *Géotechnique* 57(3):289–301

- Perras MA, Diederichs MS (2014) A review of the tensile strength of rock: concepts and testing. *Geotech Geol Eng* 32(2):525–546
- Perras MA, Ghazvinian E, Diederichs MS, Amann F, Wannenmacher H Back analysis of rock mass behavior of the Quintner Limestone at the Gonzen mine near Sargans. In: *Proceedings ISRM international symposium-EUROCK 2013, Switzerland, OnePetro*
- Qi S, Lan H, Martin D, Huang X (2019) Factors controlling the difference in Brazilian and direct tensile strengths of the Lac du Bonnet Granite. *Rock Mech Rock Eng* 53(3):1005–1019
- Rabat Á, Cano M, Tomás R, Tamayo ÁE, Alejano LR (2020a) Evaluation of strength and deformability of soft sedimentary rocks in dry and saturated conditions through needle penetration and point load tests: a comparative study. *Rock Mech Rock Eng* 53(6):2707–2726
- Rabat Á, Tomás R, Cano M (2020b) Evaluation of mechanical weakening of calcarenite building stones due to environmental relative humidity using the vapour equilibrium technique. *Eng Geol* 278:105849
- Rabat Á, Tomás R, Cano M (2021) Advances in the understanding of the role of degree of saturation and water distribution in mechanical behaviour of calcarenites using magnetic resonance imaging technique. *Constr Build Mater* 303:124420
- Rabat Á, Tomás R, Cano M, Pérez-Rey I, Siles JS, Alejano LR (2022) Influence of water content on the basic friction angle of porous limestones—experimental study using an automated tilting table. *Bull Eng Geol Environ* 81(6):223
- Rabat Á, Tomás R, Cano M (2023) Assessing water-induced changes in tensile behaviour of porous limestones by means of uniaxial direct pull test and indirect methods. *Eng Geol* 313:106962
- Ramana Y, Sarma L (1987) Split-collar, tensile test grips for short rock cores. *Eng Geol* 23(3–4):255–261
- Rodríguez P, Celestino TB (2019) Application of acoustic emission monitoring and signal analysis to the qualitative and quantitative characterization of the fracturing process in rocks. *Eng Fract Mech* 210:54–69
- Shiotani T, Ohtsu M, Ikeda K (2001) Detection and evaluation of AE waves due to rock deformation. *Constr Build Mater* 15(5):235–246
- Song K, Wang F, Yi Q, Lu S (2018) Landslide deformation behavior influenced by water level fluctuations of the Three Gorges Reservoir (China). *Eng Geol* 247:58–68
- Van E (1976) The mechanisms of strength reduction due to moisture in coal mine shales. *Int J Rock Mech Min Sci Geomech Abstr* 13(2):61–67
- Wang M, Tan C, Meng J, Yang B, Li Y (2017) Crack classification and evolution in anisotropic shale during cyclic loading tests by acoustic emission. *J Geophys Eng* 14(4):930–938
- Wang Y, Deng J, Li L, Zhang Z (2019) Micro-failure analysis of direct and flat loading Brazilian tensile tests. *Rock Mech Rock Eng* 52(11):4175–4187
- Wu C, Chen X, Hong Y, Xu R, Yu D (2018) Experimental investigation of the tensile behavior of rock with fully grouted bolts by the direct tensile test. *Rock Mech Rock Eng* 51(1):351–357
- Xie H, Ju Y, Li L (2005) Criteria for strength and structural failure of rocks based on energy dissipation and energy release principles. *Chin J Rock Mech Eng* 24(17):3003–3010
- Zang A, Christian Wagner F, Stanchits S, Dresen G, Andresen R, Haid-ekker MA (1998) Source analysis of acoustic emissions in Aue granite cores under symmetric and asymmetric compressive loads. *Geophys J Int* 135(3):1113–1130
- Zhang Z, Deng J, Zhu J, Li L (2018) An experimental investigation of the failure mechanisms of jointed and intact marble under compression based on quantitative analysis of acoustic emission waveforms. *Rock Mech Rock Eng* 51(7):2299–2307
- Zhang Z, Ma K, Li H, He Z (2022) Microscopic investigation of rock direct tensile failure based on statistical analysis of acoustic emission waveforms. *Rock Mech Rock Eng* 55(4):2445–2458
- Zheng J, Guo J, Wang J, Sun H, Deng J, Lv Q (2022) A universal elliptical disc (UED) model to represent natural rock fractures. *Int J Min Sci Technol* 32(2):261–270
- Zhou Z, Cai X, Ma D, Cao W, Chen L, Zhou J (2018) Effects of water content on fracture and mechanical behavior of sandstone with a low clay mineral content. *Eng Fract Mech* 193:47–65
- Zhu J, Deng J, Huang Y, Yu Z (2019) Experimental study on characteristic strength of saturated marble. *Chin J Rock Mech Eng* 38(6):1129–1138
- Zhu J, Deng J, Chen F, Huang Y, Yu Z (2020) Water saturation effects on mechanical and fracture behavior of marble. *Int J Geomech* 20(10):04020191
- Zhu J, Deng J, Chen F, Wang F (2022) Failure analysis of water-bearing rock under direct tension using acoustic emission. *Eng Geol* 299:106541

Publisher's Note Springer Nature remains neutral with regard to jurisdictional claims in published maps and institutional affiliations.

Springer Nature or its licensor (e.g. a society or other partner) holds exclusive rights to this article under a publishing agreement with the author(s) or other rightsholder(s); author self-archiving of the accepted manuscript version of this article is solely governed by the terms of such publishing agreement and applicable law.